Electronic Supplementary Material (ESI) for RSC Advances.

A cationic water-soluble biphen[3]arene: synthesis, host–guest complexation and fabrication of a supra-amphiphile

Jiong Zhou, Jie Yang, Zhihua Zhang, Guocan Yu*

Department of Chemistry, Zhejiang University, Hangzhou 310027, P. R. China; Fax and Tel: +86-571-8795-3189; Email address: guocanyu@zju.edu.cn.

Electronic Supplementary Information (21 pages)

1. Materials and methods

All reagents were commercially available and used as supplied without further purification. Solvents were either employed as purchased or dried according to procedures described in the literature. NMR spectra were recorded with a Bruker Avance DMX 400 spectrophotometer or a Bruker Avance DMX 500 spectrophotometer with the deuterated solvent as the lock and the residual solvent or TMS as the internal reference. Low-resolution electrospray ionization mass spectra (LRESI-MS) were obtained on a Bruker Esquire 3000 Plus spectrometer (Bruker-Franzen Analytik GmbH Bremen, Germany) equipped with an ESI interface and an ion trap analyzer. High-resolution electrospray ionization mass spectra (HRESI-MS) were obtained on a Bruker 7-Tesla FT-ICR mass spectrometer equipped with an electrospray source (Billerica, MA, USA). MALDI-TOF-MS spectra were performed on a AXIMA Performance-MALDI TOF/TOF (Matrix: 2,5-dihydroxy-benzoic acid). The melting points were collected on a SHPSIC WRS-2 automatic melting point apparatus. The critical aggregation concentration (CAC) values of **G** and **H⊃G** were determined on a DDS-307 instrument. Transmission electron microscopy (TEM) investigations were carried out on a JEM-1200EX instrument. Dynamic light scattering measurements were performed on a goniometer ALV/CGS-3 using a UNIPHASE He-Ne laser operating at 632.8 nm. The fluorescence experiments were conducted on a RF-5301 spectrofluorophotometer (Shimadzu Corporation, Japan).

*2. Synthesis of cationic water-soluble biphen[3]arene **H***

Scheme S1. Synthetic route to cationic water-soluble biphen[3]arene **H**.

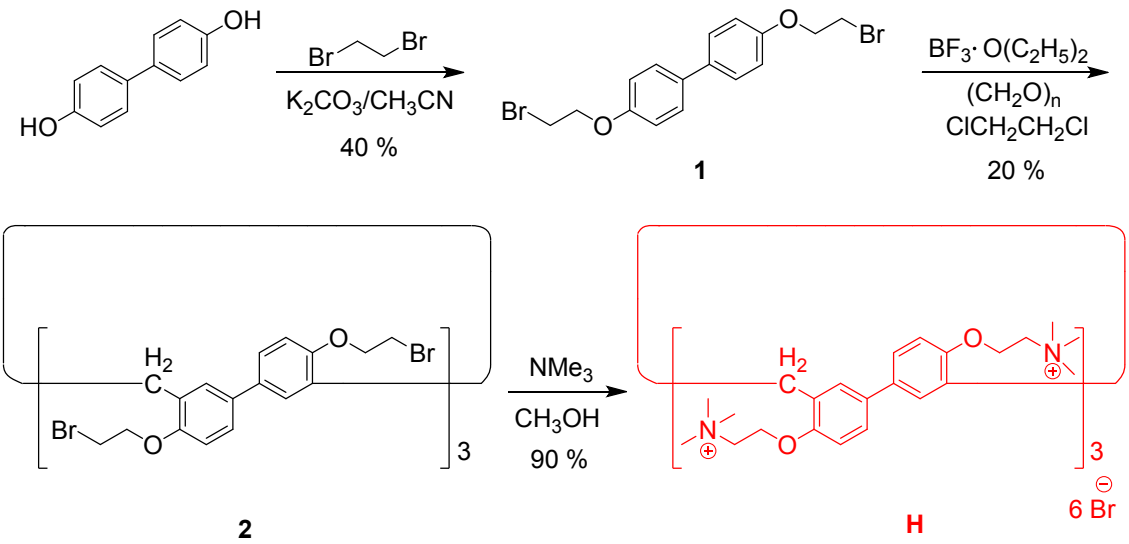

*2.1. Synthesis of compound **1**[S1]*

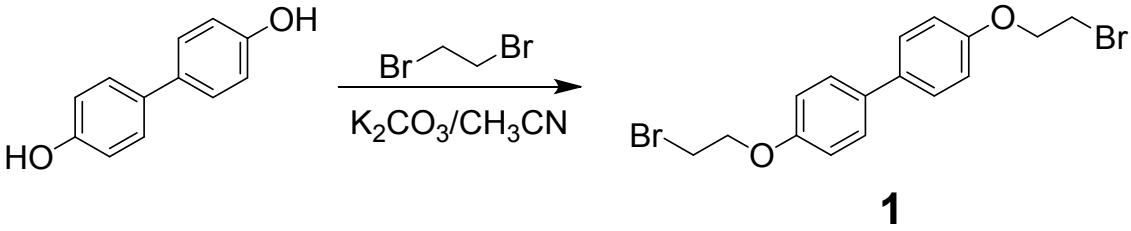

A mixture of 1,2-dibromoethane (18.8 g, 100 mmol), 4,4'-biphenol (1.86 g, 10.0 mmol), and K_2CO_3 (5.52 g, 40.0 mmol) in 150 mL CH_3CN was refluxed under N_2 for 24 h. Then the reaction mixture was cooled to room temperature and filtered. The filter cake was washed with dichloromethane (2 × 60 mL). The filtrate was concentrated under vacuum, and then the residue was purified by column chromatography on silica gel with dichloromethane/petroleum ether (1:1 *v*/*v*) as the eluent to get product **1** as a white solid (1.60 g, 40 %). The ^{1}H NMR spectrum of **1** is shown in Fig. S1. ^{1}H NMR (400 MHz, chloroform-*d*, 293 K) δ (ppm): 7.48 (d, J = 8 Hz, 4H), 6.97 (d, J = 8 Hz, 4H), 4.33 (t, J = 6 Hz, 4H), 3.67 (t, J = 6 Hz, 4H).

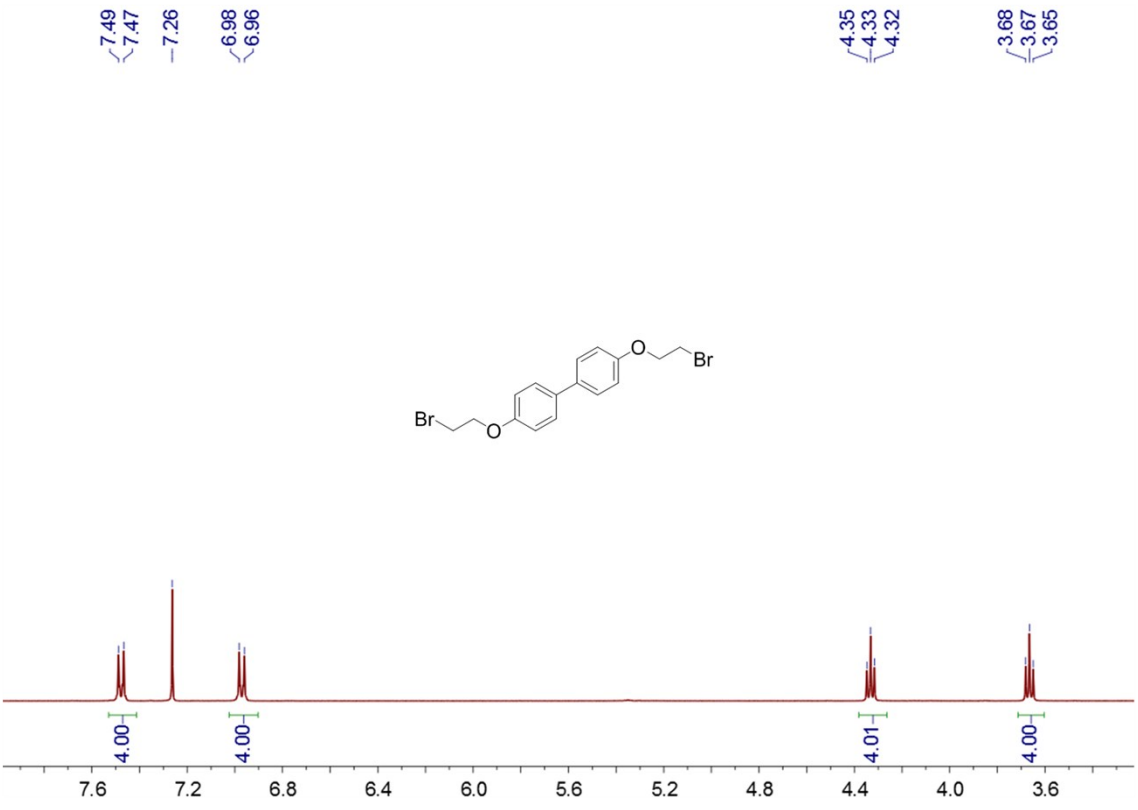

Fig. S1 ^{1}H NMR spectrum (400 MHz, chloroform-*d*, 293K) of **1**.

*2.2. Synthesis of compound **2***

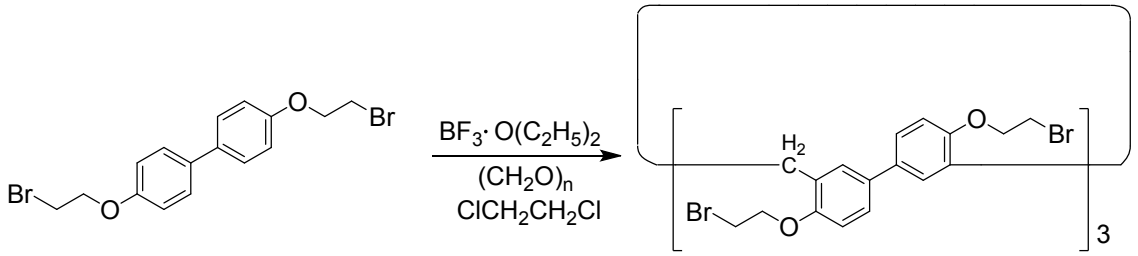

1 **2**

To the solution of **1** (1.00 g, 2.50 mmol) in 1, 2-dichloroethane (50 mL), paraformaldehyde (0.0750 g, 2.50 mmol) was added. The suspension was stirred at 25 °C for 30 min to crush the large paraformaldehyde particles. Then boron trifluoride diethyl etherate ($BF_3{\cdot}O(C_2H_5)_2$, 0.355 g, 2.50 mmol) was added to the solution. After continuing stirred at 25 °C for 3.5 h, the reaction was quenched by addition of water. The organic phase was separated and the crude product was purified by column chromatography (petroleum ether/dichloromethane, v/v 1:1) to get **2** as a white solid (0.206 g, 20 %), mp: 235.2−236.5 ºC. The ^{1}H NMR spectrum of **2** is shown in Fig. S2. ^{1}H NMR (400 MHz, chloroform-*d*, 293 K) δ (ppm): 7.29 (d, J = 8 Hz, 6H), 7.06 (s, 6H), 6.84 (d, J = 8 Hz, 6H), 4.26 (t, J = 6 Hz, 12H), 4.04 (s, 6H), 3.56 (t, J = 6 Hz, 12H). The ^{13}C NMR spectrum of **2** is shown in Fig. S3. ^{13}C NMR (100 MHz, chloroform-*d*, 293 K) δ (ppm): 155.09, 134.08, 130.17, 128.93, 125.55, 112.32, 68.46, 29.41 and 29.04.

MALDI-TOF-MS is shown in Fig. S4: *m*/*z* calcd for $[M + H]^+$ $C_{51}H_{49}Br_6O_6^+$, 1236.8568; found 1236.857. HRESIMS: *m*/*z* of $C_{51}H_{42}O_{18}Na$ 1258.8547 $[M + Na]^+$, 619.5259 $[M + 2H]^{2+}$.

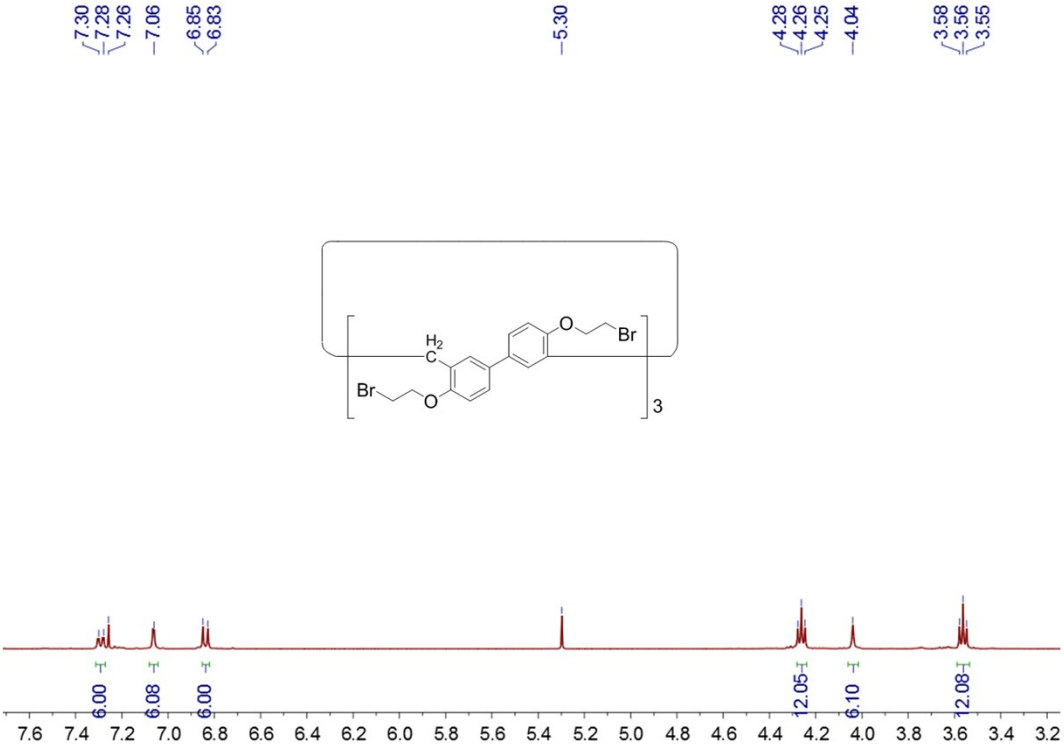

Fig. S2 ^{1}H NMR spectrum (400 MHz, chloroform-*d*, 293K) of **2**.

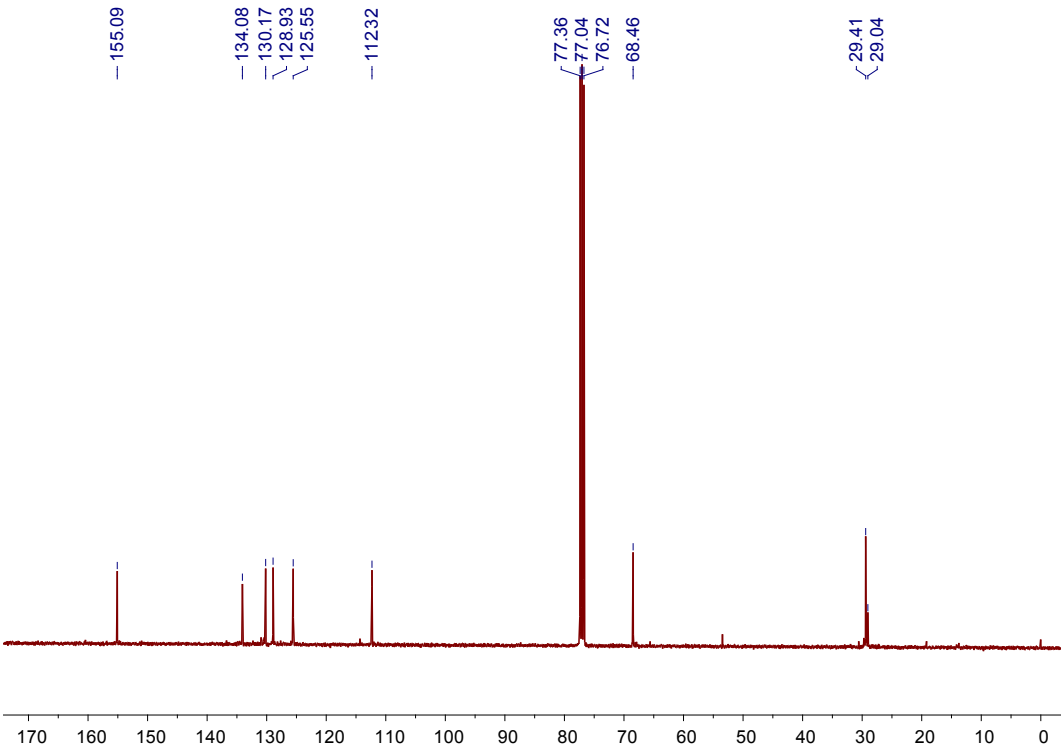

Fig. S3 ^{13}C NMR spectrum (100 MHz, chloroform-*d*, 293K) of **2**.

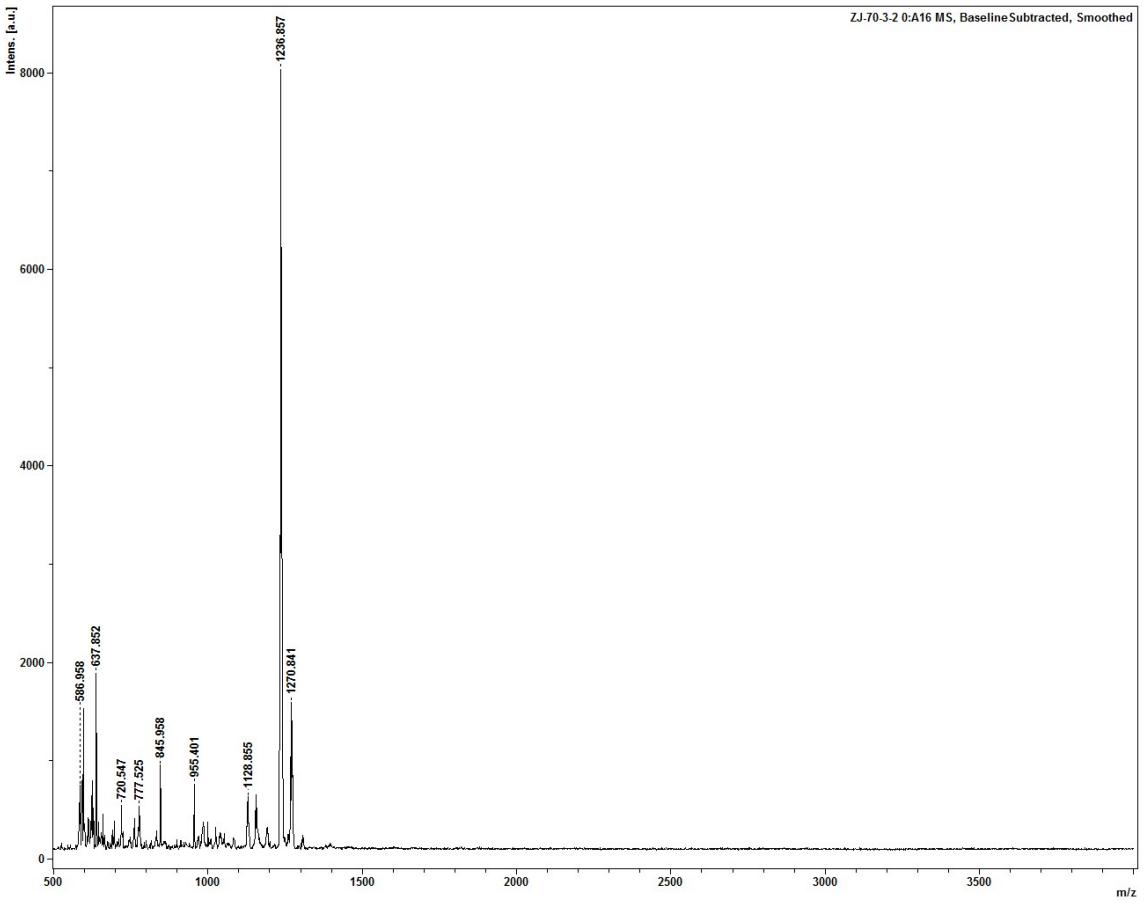

Fig. S4 MALDI-TOF-MS of **2**. Assignment of the main peak: *m*/*z* 1236.857 $[M + H]^+$.

*2.3. Synthesis of compound **H***

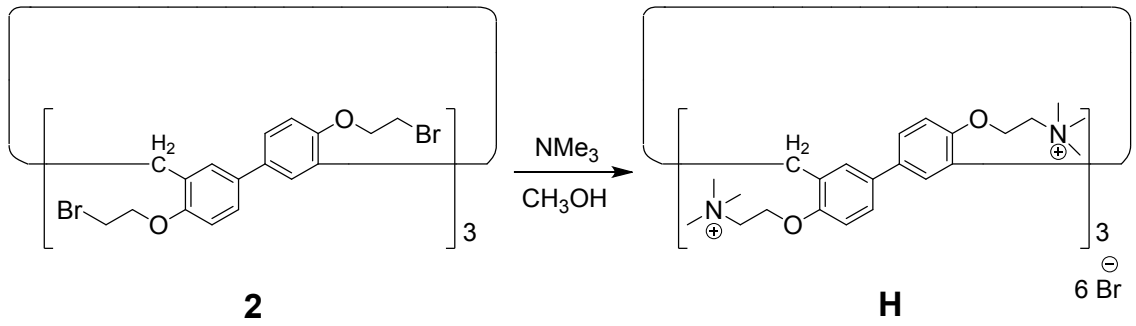

2 **H**

Compound **2** (0.124 g, 0.100 mmol) and trimethylamine (33 % in methanol, 5 mL, 18.5 mmol) were added to methanol (20 mL). The solution was refluxed overnight. Then the solvent was removed by evaporation, deionized water (20 mL) was added. After filtration, a clear solution was got. Water was then removed by rotary evaporation to gain **H** as a white powder (143 mg, 90 %), mp: > 300 ºC. The ^{1}H NMR spectrum of **H** is shown in Fig. S5. ^{1}H NMR (400 MHz, D_2O, 293 K) δ (ppm): 7.42 (d, J = 8 Hz, 6H), 7.06 (d, J = 8 Hz, 6H), 7.01 (s, 6H), 4.45 (s, 12H), 3.95 (s, 6H), 3.74 (s, 12H), 3.05 (s, 54H). The ^{13}C NMR spectrum of **H** is shown in Fig. S6. ^{13}C NMR (100 MHz, D_2O, 293 K) δ (ppm): 157.35, 137.00, 132.04, 131.79, 129.31, 115.14, 68.18, 65.01, 62.54 and 56.79. LRESIMS is shown in Fig. S7: *m*/*z* 318.3 $[M - 4Br]^{4+}$. MALDI-TOF-MS: *m*/*z* of $C_{69}H_{102}Br_5N_6O_6$ 1510.778 $[M - Br]^+$. HRESIMS: *m*/*z* of 318.2960 $[M - 4Br]^{4+}$.

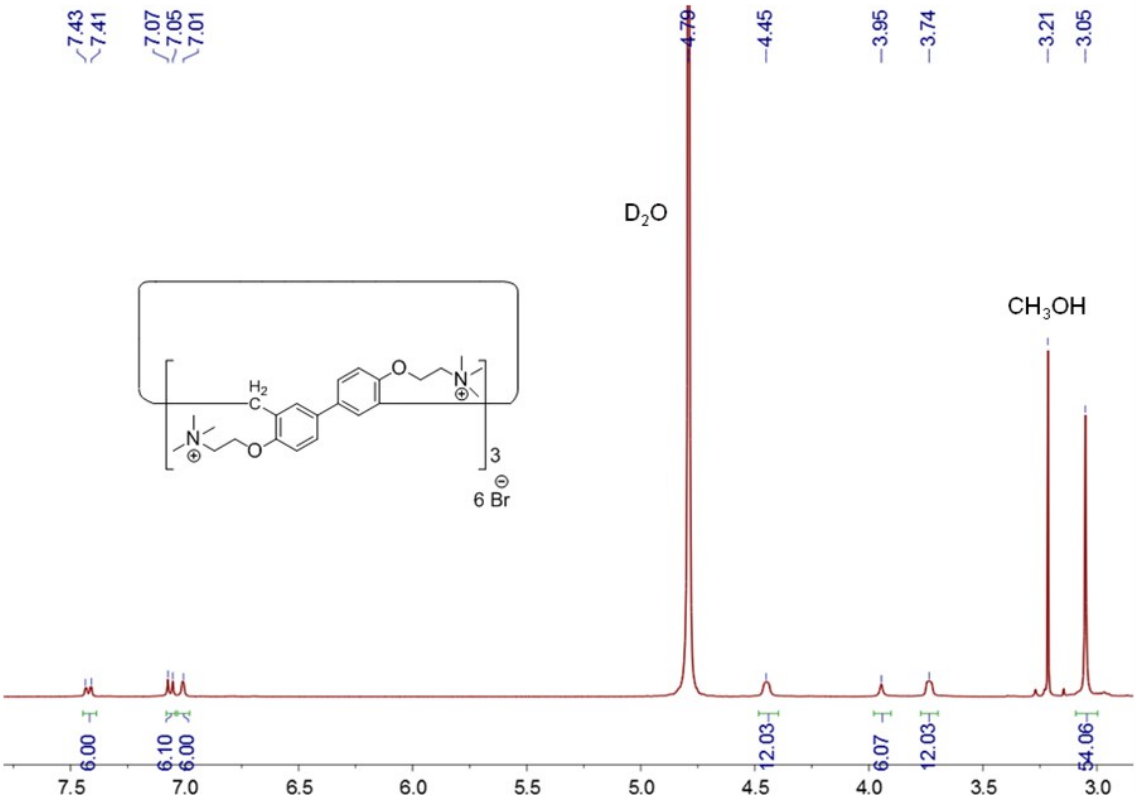

Fig. S5 ^{1}H NMR spectrum (400 MHz, D_2O, 293K) of **H**.

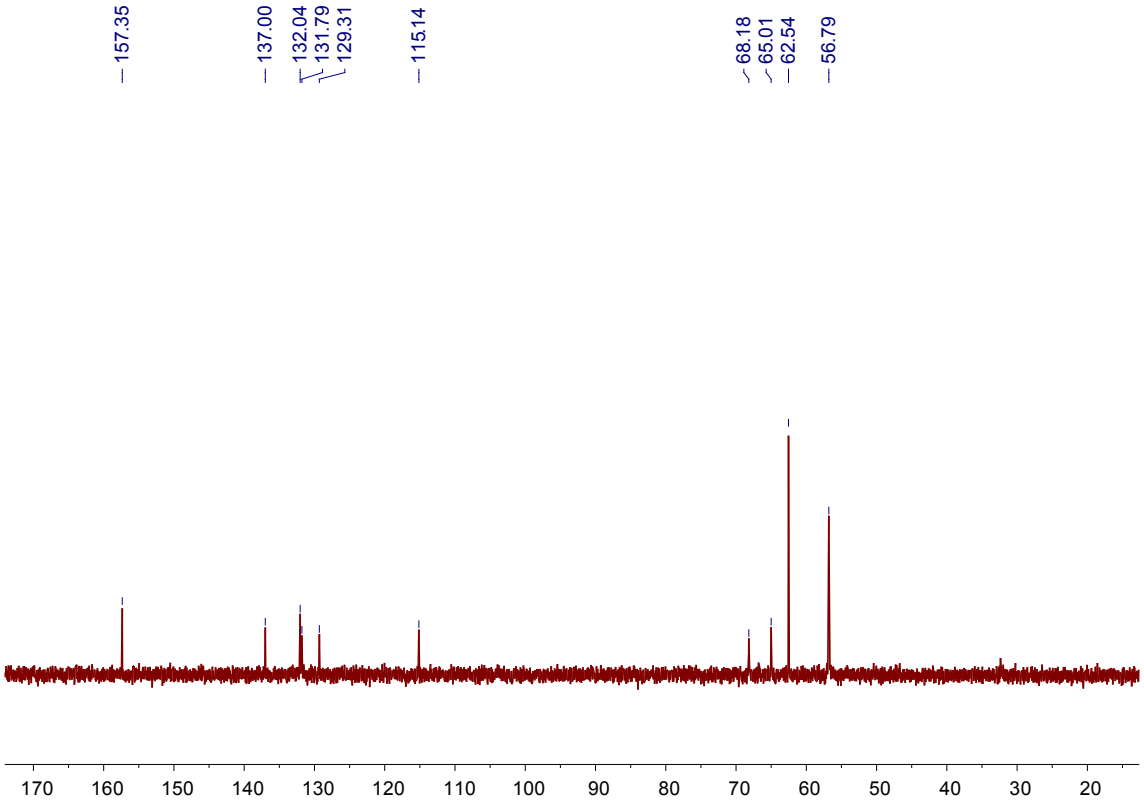

Fig. S6 ^{13}C NMR spectrum (100 MHz, D_2O, 293K) of **H**.

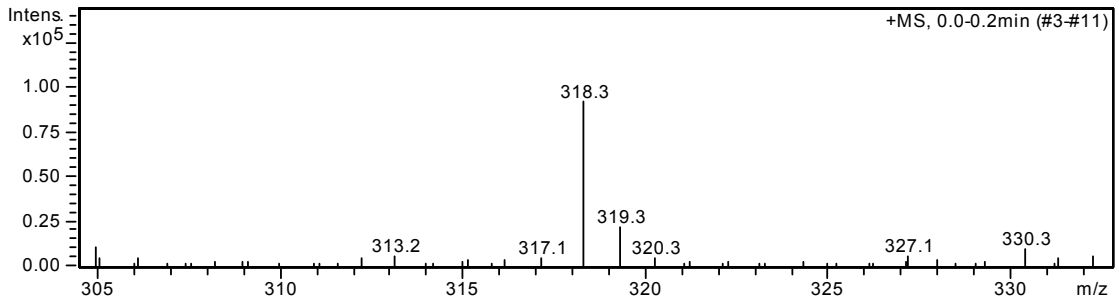

Fig. S7 Electrospray ionization mass spectrum of **H**. Assignment of the main peak: *m*/*z* 318.3 $[M - 4Br]^{4+}$.

*3. ^{1}H NMR investigations between **H** and compounds **G2**, **G3***

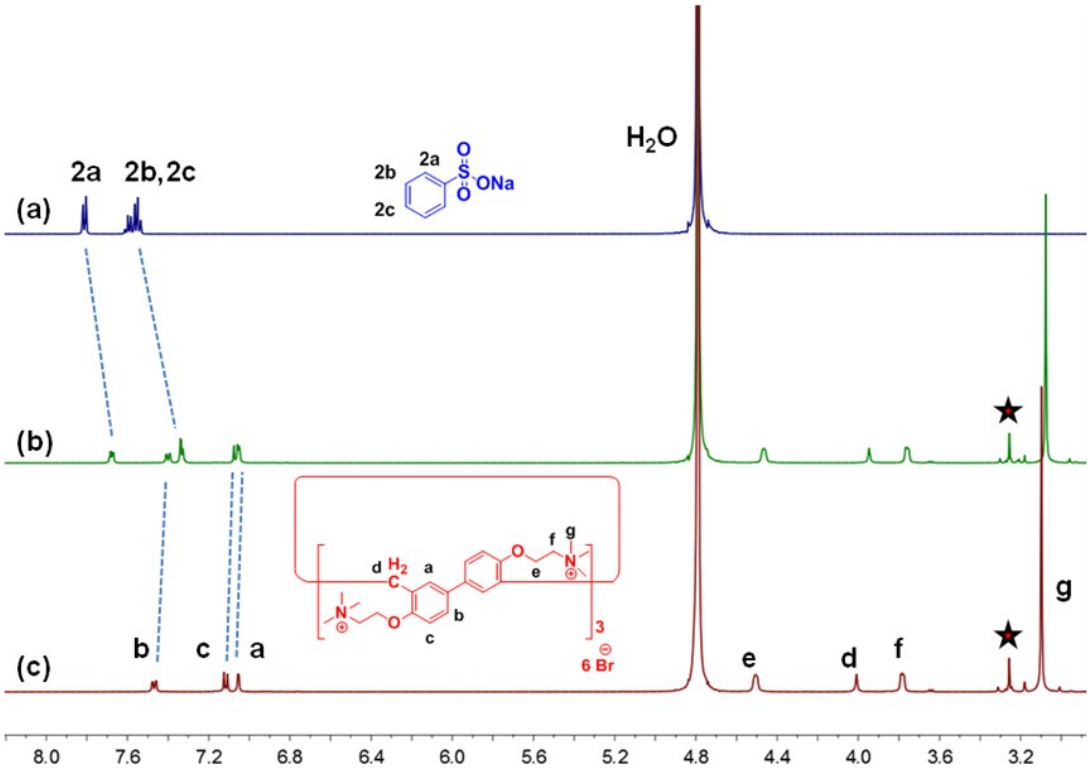

Fig. S8 ^{1}H NMR spectra (400 MHz, D_2O, 293 K) of (a) 2.00 mM **G2**; (b) 2.00 mM **G2** and 2.00 mM **H**; (c) 2.00 mM **H**. (The asterisk represents the protons related to methanol)

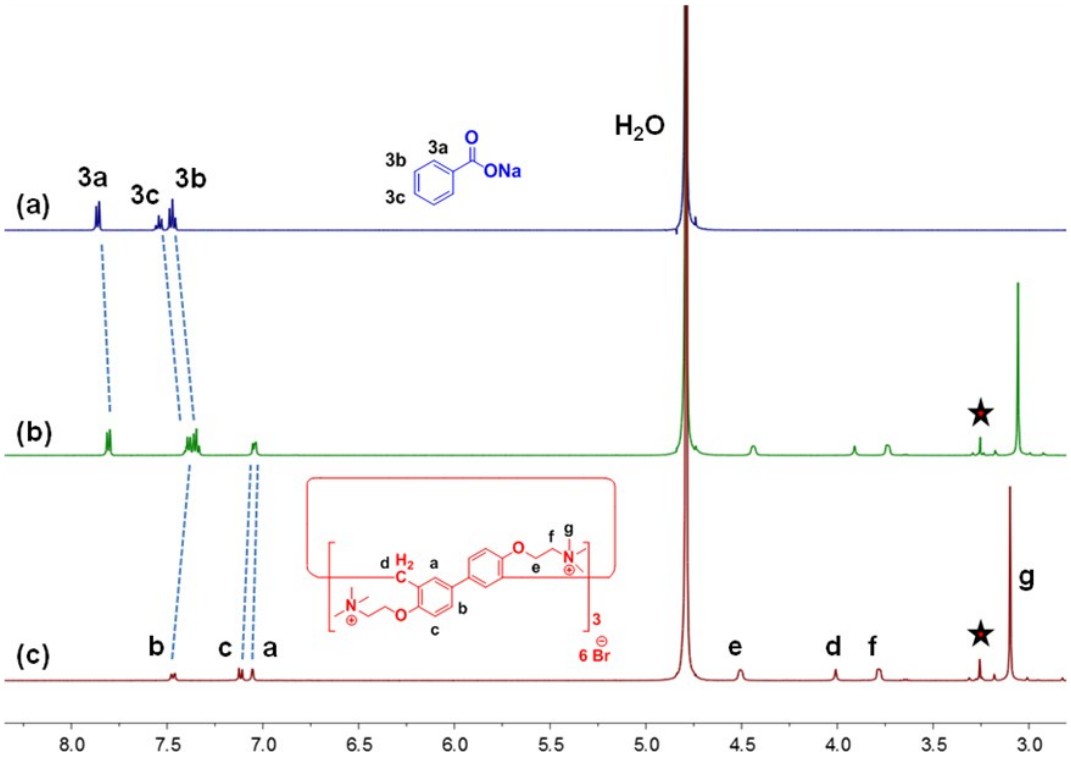

Fig. S9 ^{1}H NMR spectra (400 MHz, D_2O, 293 K) of (a) 2.00 mM **G3**; (b) 2.00 mM **G3** and 2.00 mM **H**; (c) 2.00 mM **H**. (The asterisk represents the protons related to methanol)

*4. 2D NOESY spectrum between **H** and compounds **G1**, **G2**, **G3***

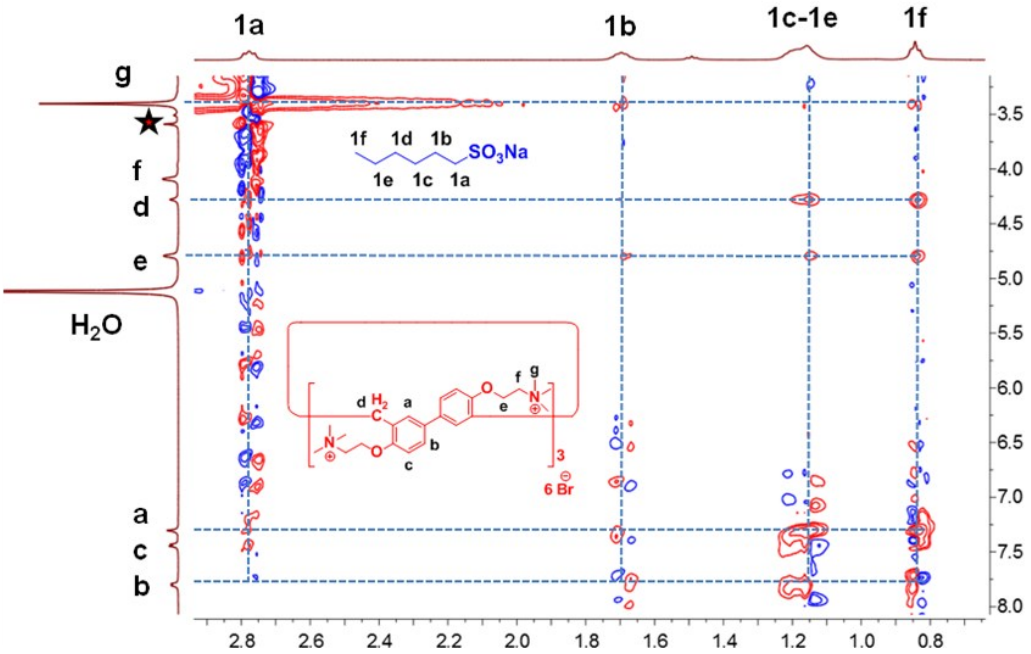

Fig. S10 2D NOESY NMR (500 MHz, D_2O, 293 K) spectrum of a solution of **H** (10.0 mM) and **G1** (10.0 mM). (The asterisk represents the protons related to methanol)

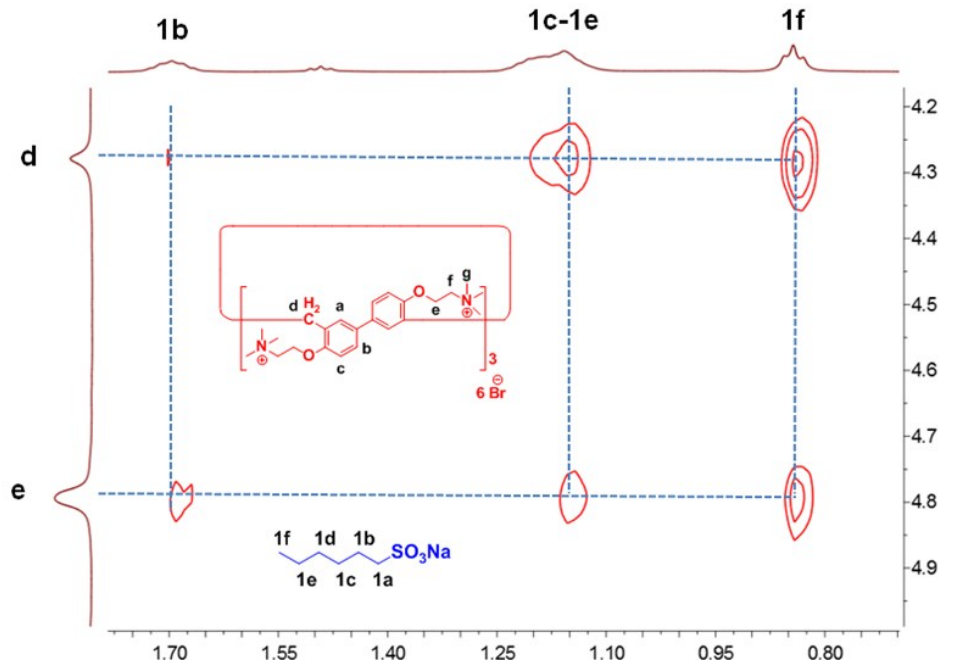

Fig. S11 Partial 2D NOESY NMR (500 MHz, D_2O, 293 K) spectrum of a solution of **H** (10.0 mM) and **G1** (10.0 mM).

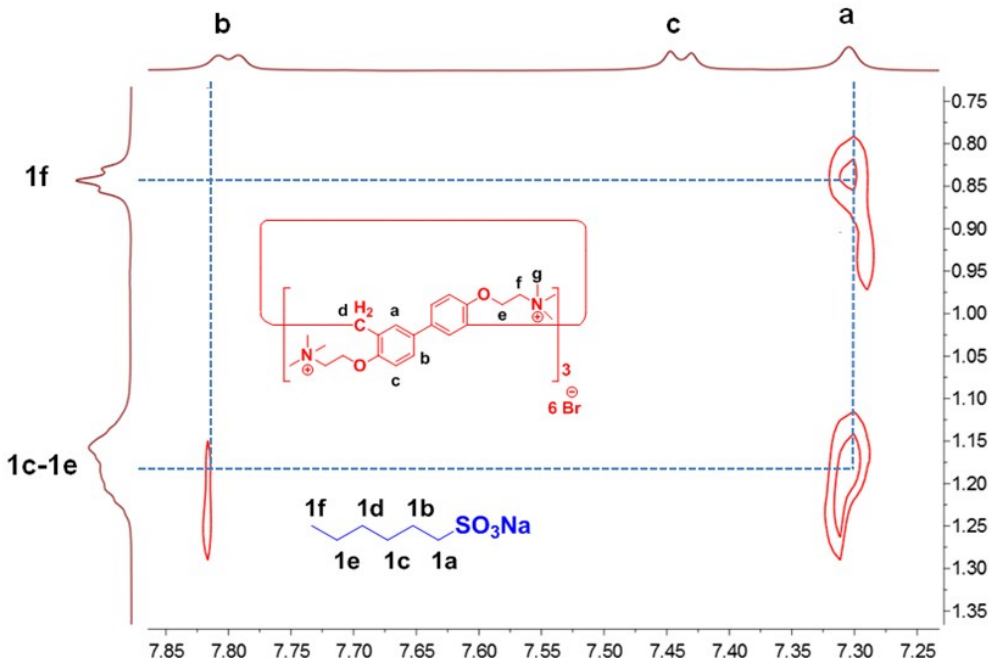

Fig. S12 Partial 2D NOESY NMR (500 MHz, D_2O, 293 K) spectrum of a solution of **H** (10.0 mM) and **G1** (10.0 mM).

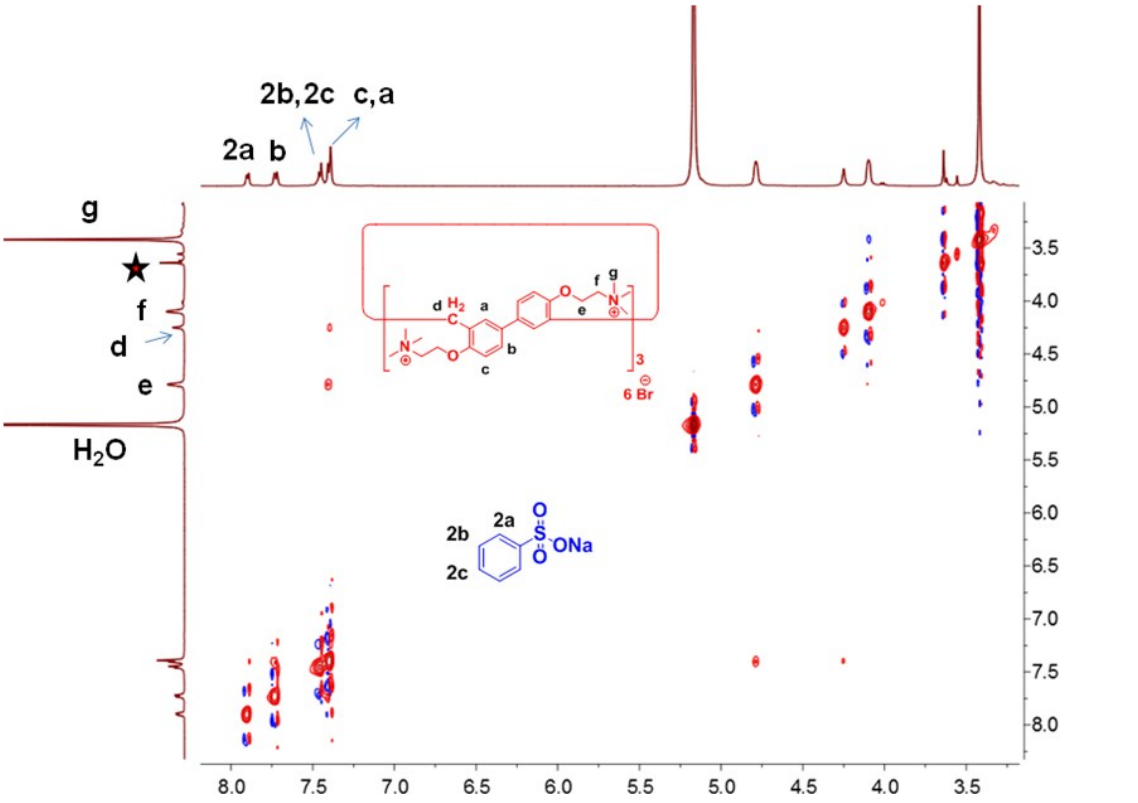

Fig. S13 2D NOESY NMR (500 MHz, D_2O, 293 K) spectrum of a solution of **H** (10.0 mM) and **G2** (10.0 mM). (The asterisk represents the protons related to methanol)

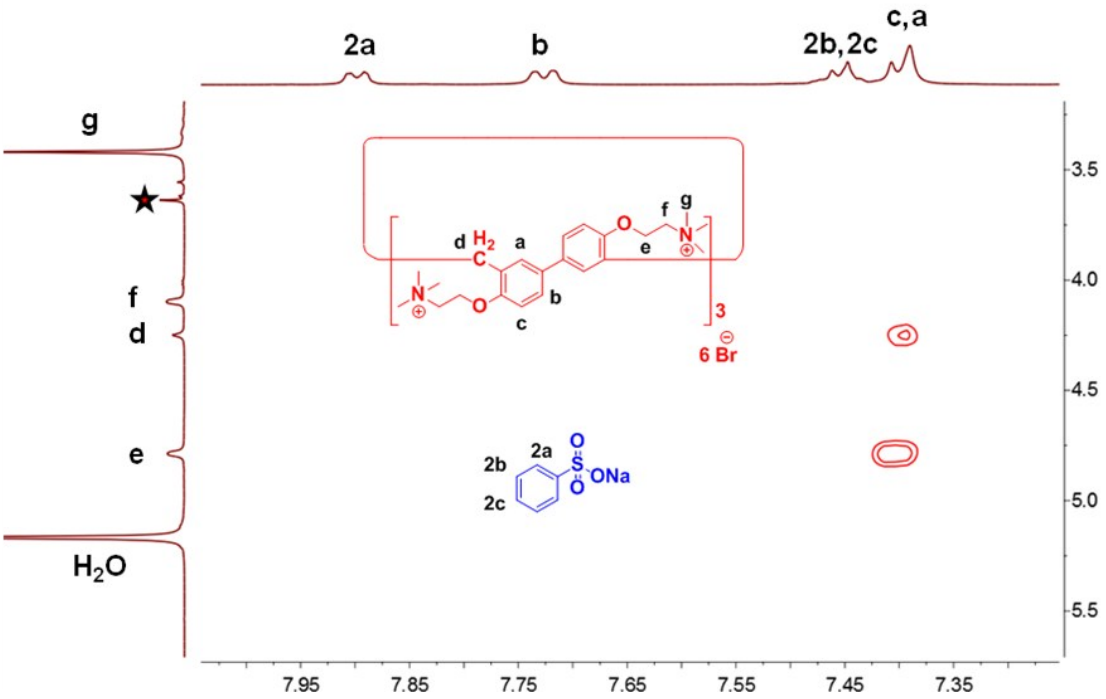

Fig. S14 Partial 2D NOESY NMR (500 MHz, D_2O, 293 K) spectrum of a solution of **H** (10.0 mM) and **G2** (10.0 mM). (The asterisk represents the protons related to methanol)

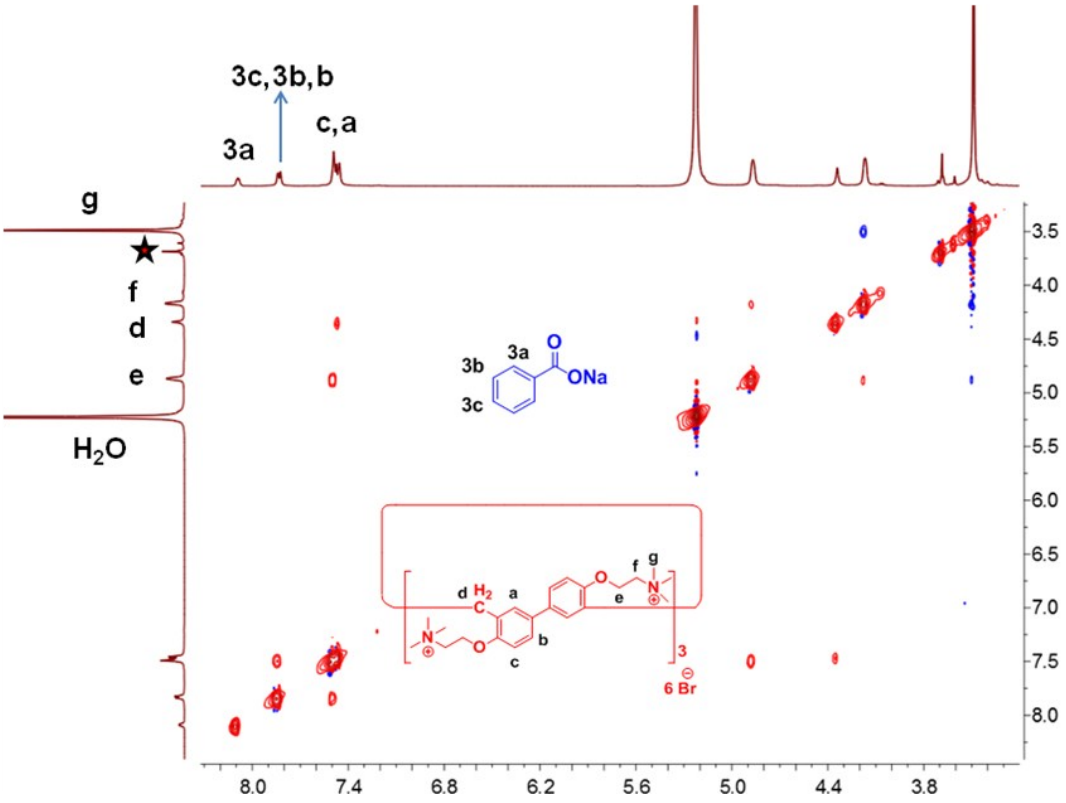

Fig. S15 2D NOESY NMR (500 MHz, D_2O, 293 K) spectrum of a solution of **H** (10.0 mM) and **G3** (10.0 mM). (The asterisk represents the protons related to methanol)

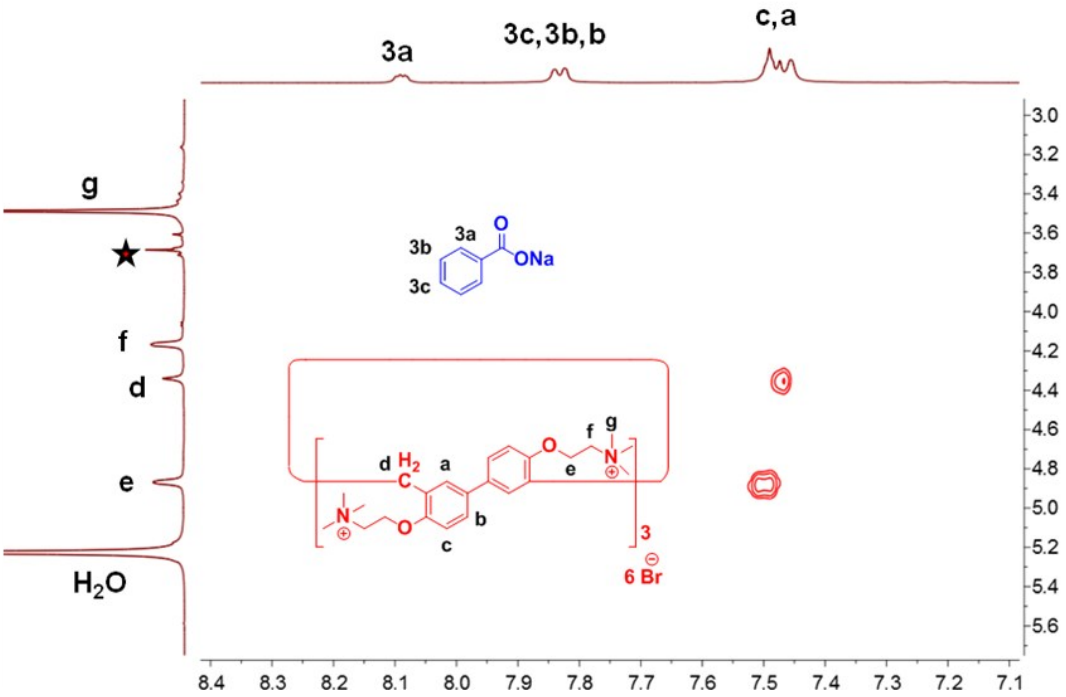

Fig. S16 Partial 2D NOESY NMR (500 MHz, D_2O, 293 K) spectrum of a solution of **H** (10.0 mM) and **G3** (10.0 mM). (The asterisk represents the protons related to methanol)

*5. Association constant and stoichiometry determination for the complexation between **H** and compounds **G1**, **G2**, **G3***

To determine the association constant and stoichiometry for the complexation between **H** and **G1** (or **G2** or **G3**), ^{1}H NMR titration was done with solutions which had a constant concentration of the host **H** (1.00 mM) and varying concentrations of the guest **G1** (or **G2** or **G3**). By a non-linear curve-fitting method, the association constant (K_a) of **H⊃G1** (or **H⊃G2** or **H⊃G3**) was determined. By a mole ratio plot, 1:1 stoichiometry was obtained for the complexation between **H** and **G1** (or **G2** or **G3**).

The non-linear curve-fitting was based on the equation:[S2]

$$\Delta\delta = (\Delta\delta_\infty/[H]_0)\ (0.5[G]_0 + 0.5([H]_0+1/K_a) - (0.5\ ([G]_0^2 + (2[G]_0\ (1/K_a - [H]_0)) + (1/K_a + [H]_0)^2)^{0.5})) \quad \text{(Eq. S1)}$$

Where $\Delta\delta$ is the chemical shift change of H_a (or H_d) on **H**, $\Delta\delta_\infty$ is the chemical shift change of H_a (or H_d) when the host **H** is completely complexed, $[G]_0$ is the initial concentration of the guest **G1** (or **G2** or **G3**), and $[H]_0$ is the fixed initial concentration of the host **H**.

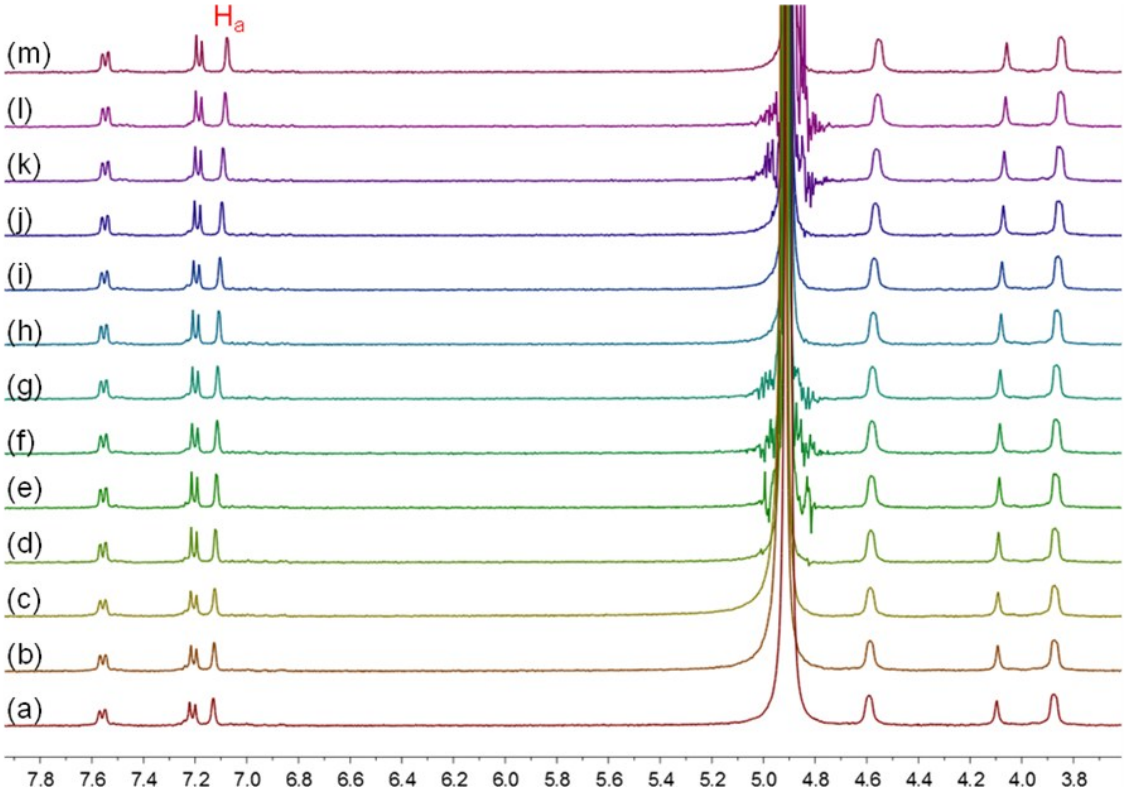

Fig. S17 Partial ^{1}H NMR spectra (400 MHz, D_2O, 293K) of **H** at a concentration of 1.00 mM upon addition of **G1**: (a) 0.00 mM; (b) 0.031 mM; (c) 0.071 mM; (d) 0.189 mM; (e) 0.307 mM; (f) 0.418 mM; (g) 0.465 mM; (h) 0.568 mM; (i) 0.821 mM; (j) 1.21 mM; (k) 1.61 mM; (l) 2.41 mM; (m) 3.47 mM.

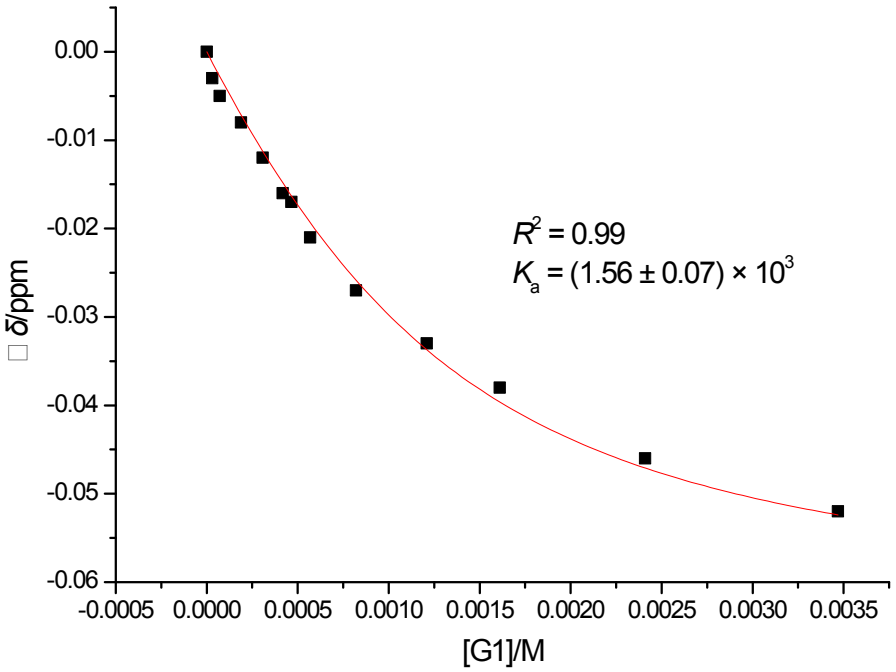

Fig. S18 The chemical shift changes of H_a on **H** upon addition of **G1**. The red solid line was obtained from the non-linear curve-fitting using Eq. S1.

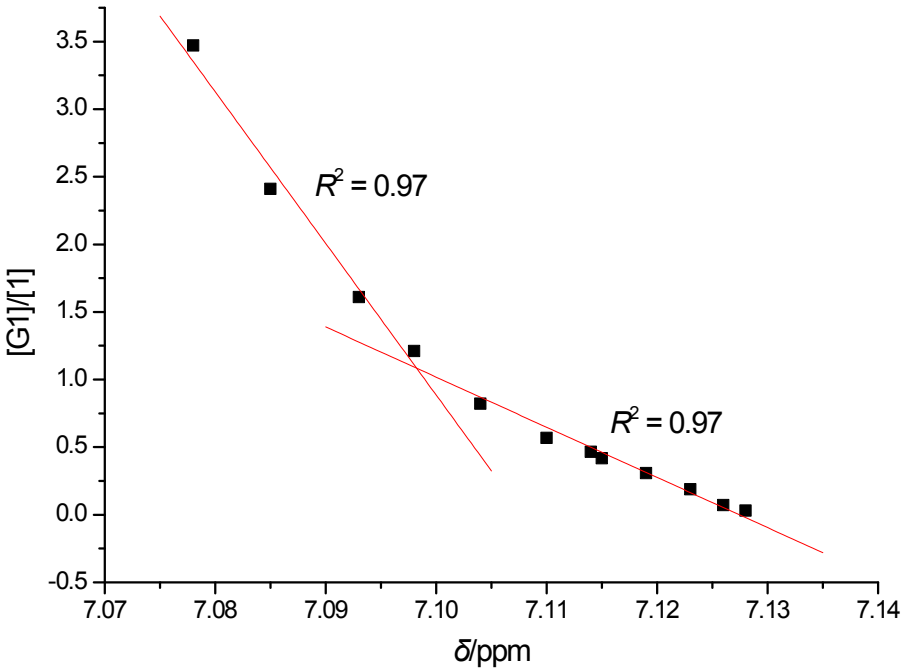

Fig. S19 Mole ratio plot for **H** and **G1**, indicating a 1:1 stoichiometry.

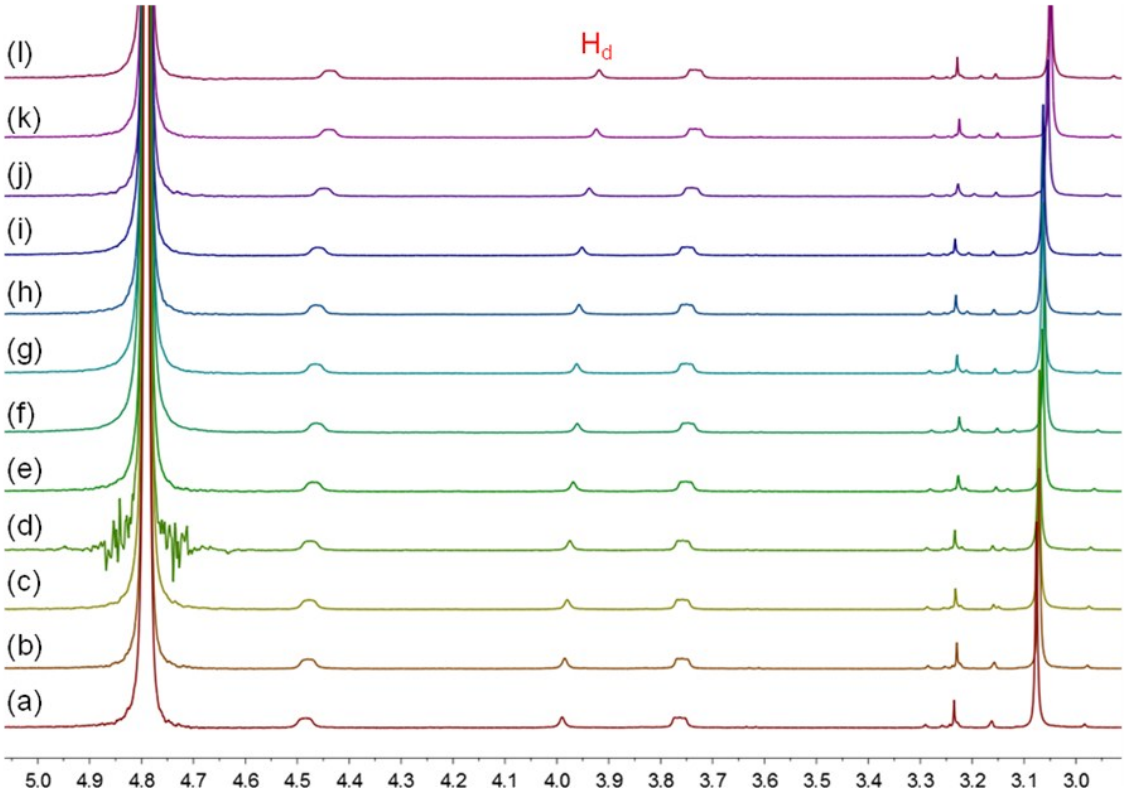

Fig. S20 Partial ^{1}H NMR spectra (400 MHz, D_2O, 293K) of **H** at a concentration of 1.00 mM upon addition of **G2**: (a) 0.00 mM; (b) 0.198 mM; (c) 0.449 mM; (d) 0.678 mM; (e) 0.951 mM; (f) 1.31 mM; (g) 1.61 mM; (h) 1.88 mM; (i) 2.25 mM; (j) 3.01 mM; (k) 3.93 mM; (l) 4.96 mM.

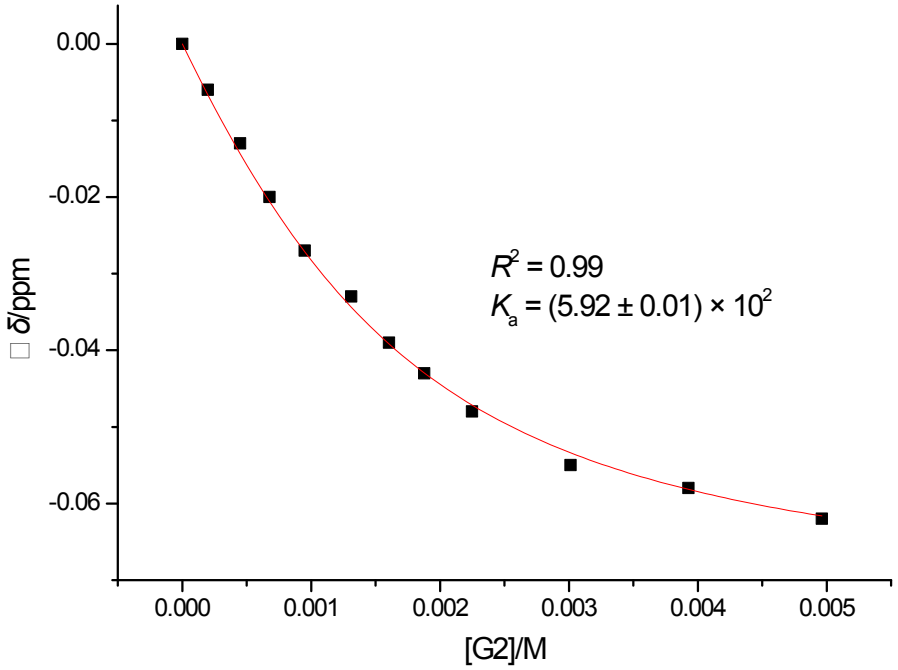

Fig. S21 The chemical shift changes of H_d on **H** upon addition of **G2**. The red solid line was obtained from the non-linear curve-fitting using Eq. S1.

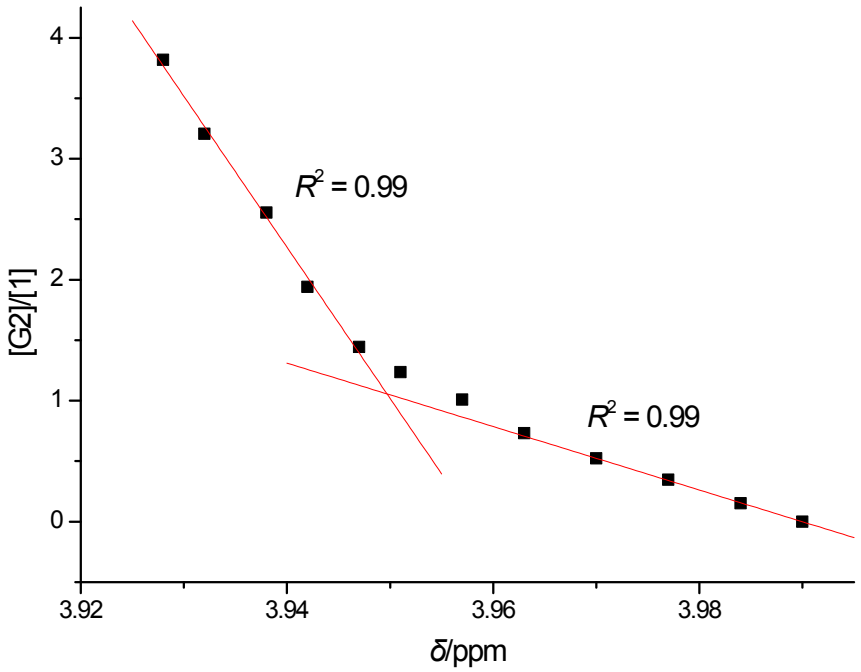

Fig. S22 Mole ratio plot for **H** and **G2**, indicating a 1:1 stoichiometry.

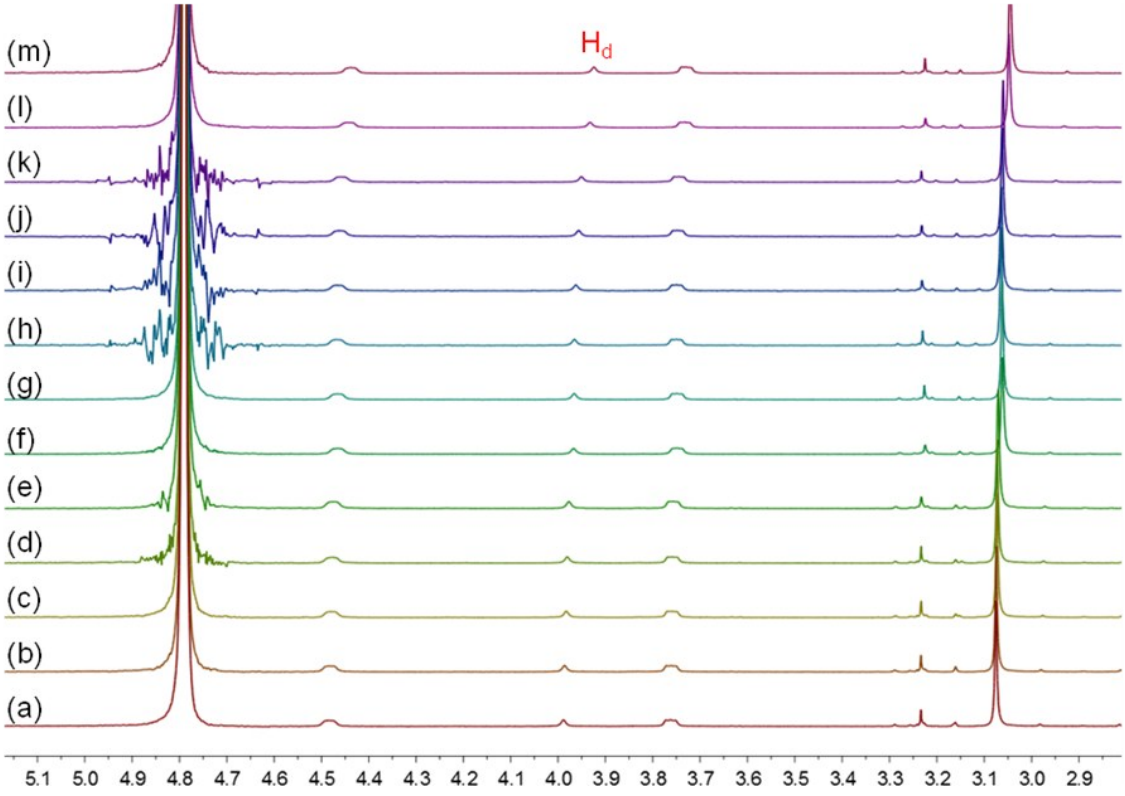

Fig. S23 Partial ^{1}H NMR spectra (400 MHz, D_2O, 293K) of **H** at a concentration of 1.00 mM upon addition of **G3**: (a) 0.00 mM; (b) 0.420 mM; (c) 0.730 mM; (d) 1.01 mM; (e) 1.24 mM; (f) 1.59 mM; (g) 1.92 mM; (h) 2.24 mM; (i) 2.68 mM; (j) 3.08 mM; (k) 3.52 mM; (l) 4.35 mM; (m) 5.27 mM.

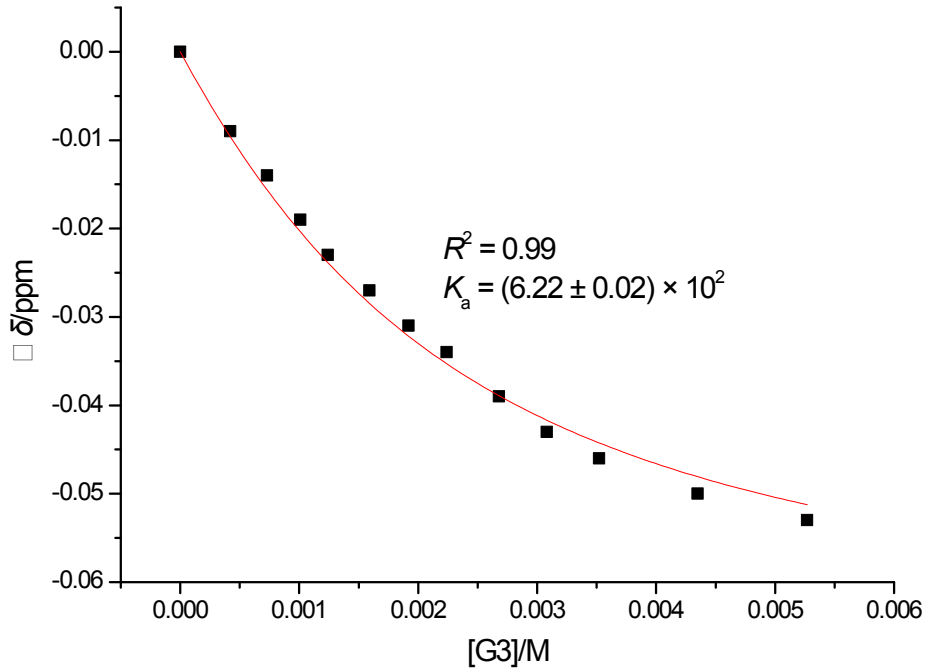

Fig. S24 The chemical shift changes of H_d on **H** upon addition of **G3**. The red solid line was obtained from the non-linear curve-fitting using Eq. S1.

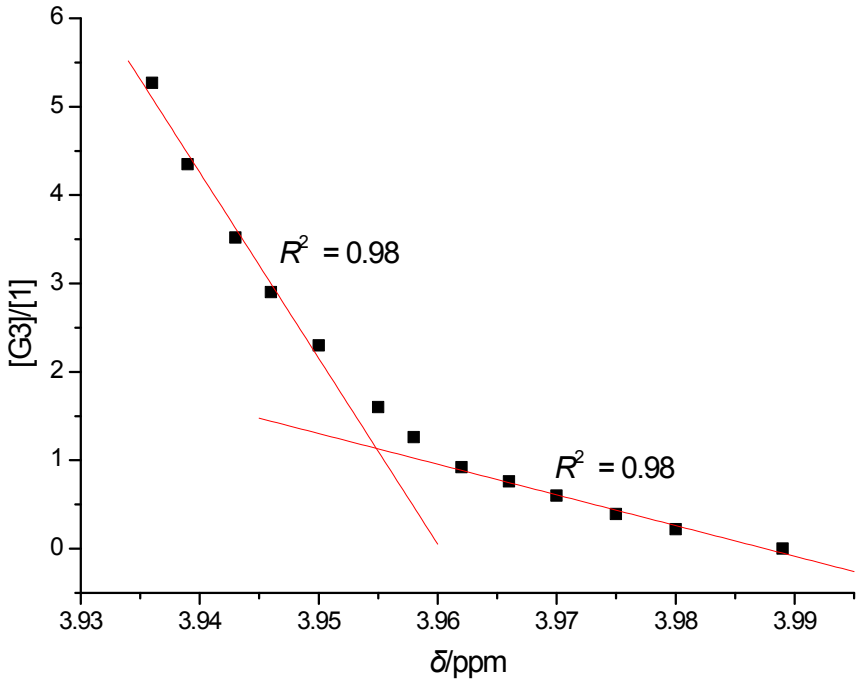

Fig. S25 Mole ratio plot for **H** and **G3**, indicating a 1:1 stoichiometry.

*6. Electrospray ionization mass spectrum of a solution of **H** and model compound **G1** in water*

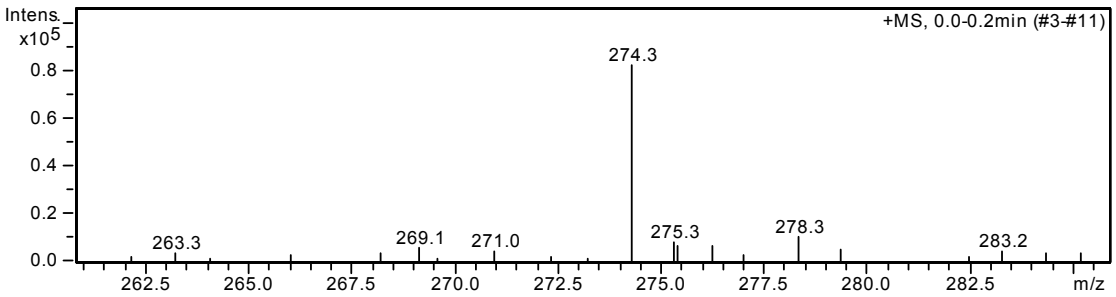

Fig. S26 Electrospray ionization mass spectrometry of a solution of **H** with **G1** in water. Assignment of main peaks: *m*/*z* 274.3 [**H⊃G1** − 5Br]$^{5+}$.

*7. Critical aggregation concentration (CAC) determination of **G** and **H⊃G***

Some parameters such as the conductivity, fluorescence intensity, osmotic pressure and surface tension of the solution change sharply around the critical aggregation concentration. The dependence of the solution conductivity on the solution concentration is used to determine the critical aggregation concentration. Typically, the slope of conductivity versus the concentration below CAC is steeper than the slope above the CAC. Therefore, the junction of the conductivity-concentration plot represents the CAC value. To measure the CAC values of **G** and **H⊃G**, the conductivities of the solutions at different concentrations (from 0 to 0.171 mM) were determined. By plotting the conductivity versus the concentration, we estimated the CAC values of **G** and **H⊃G**.

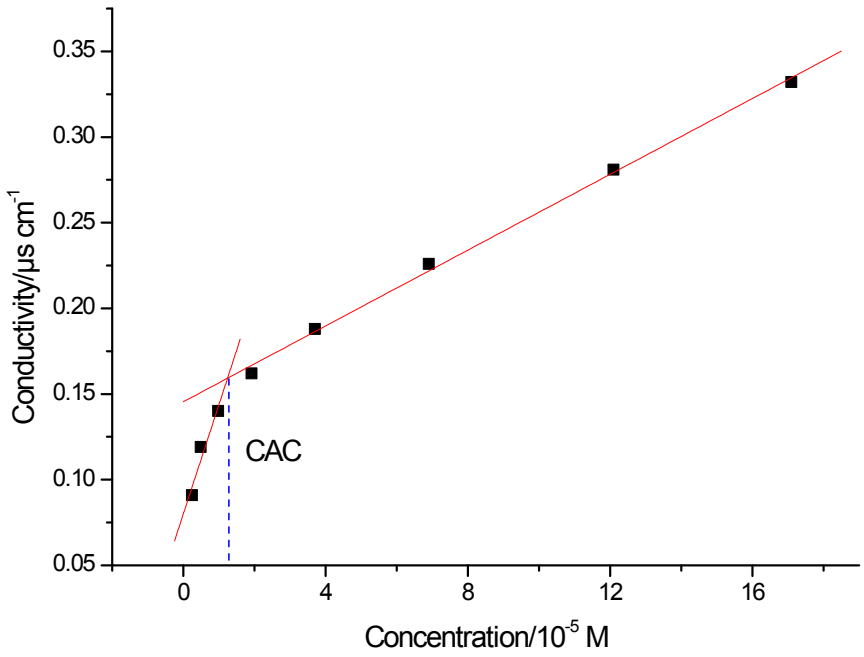

Fig. S27 The concentration-dependent conductivity of **G**. The critical aggregation concentration was determined to be 1.24 × 10^{-5} M.

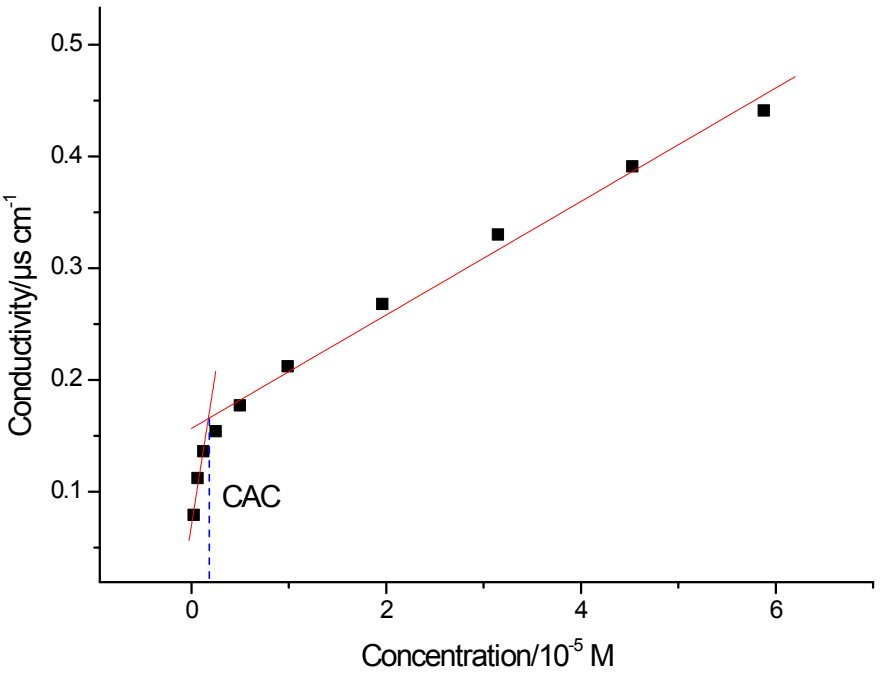

Fig. S28 The concentration-dependent conductivity of **H⊃G**. The critical aggregation concentration (CAC) was determined to be 1.69×10^{-6} M.

*8. Dynamic light scattering (DLS) results of **G** and **H⊃G***

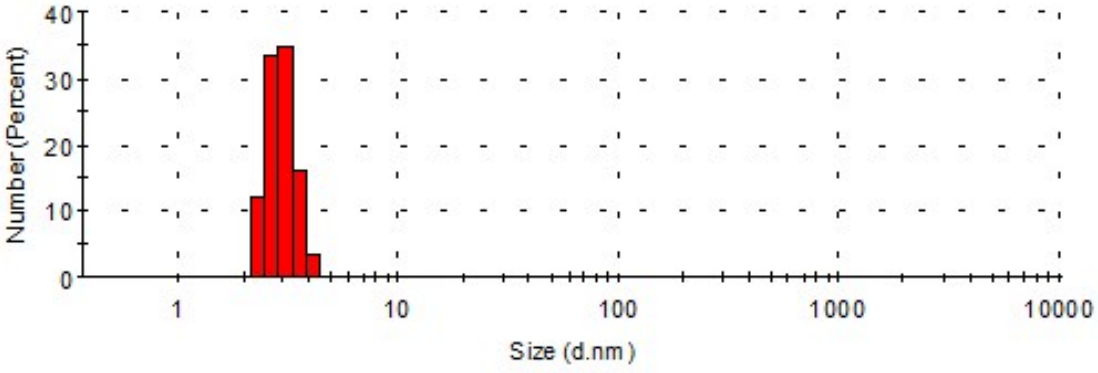

Fig. S29 DLS result of **G** with an aqueous solution of 5.00×10^{-4} M.

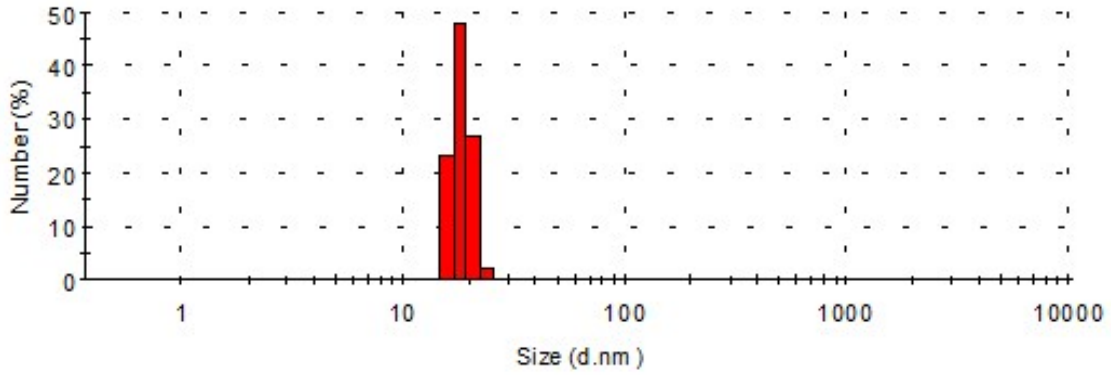

Fig. S30 DLS result of **H⊃G** with an aqueous solution of 3.33×10^{-4} M.

*9. Zeta potential results of **G** and **H⊃G***

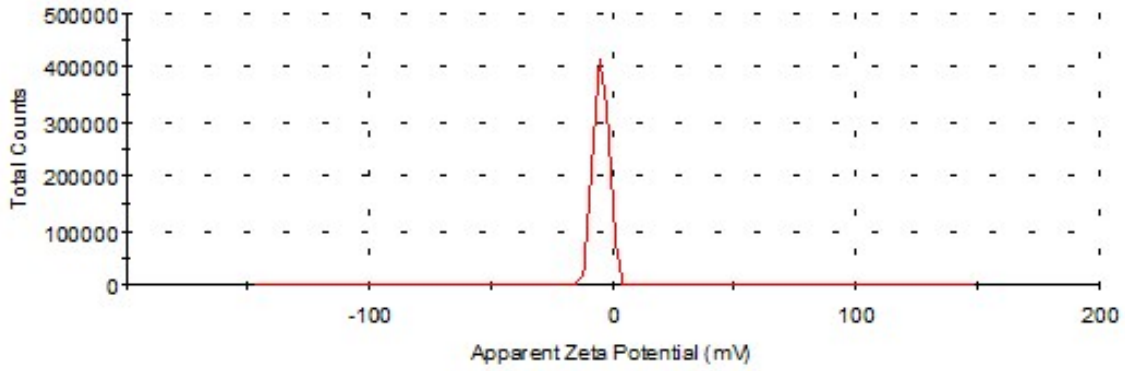

Fig. S31 Zeta potential result of **G** with an aqueous solution of 5.00×10^{-4} M.

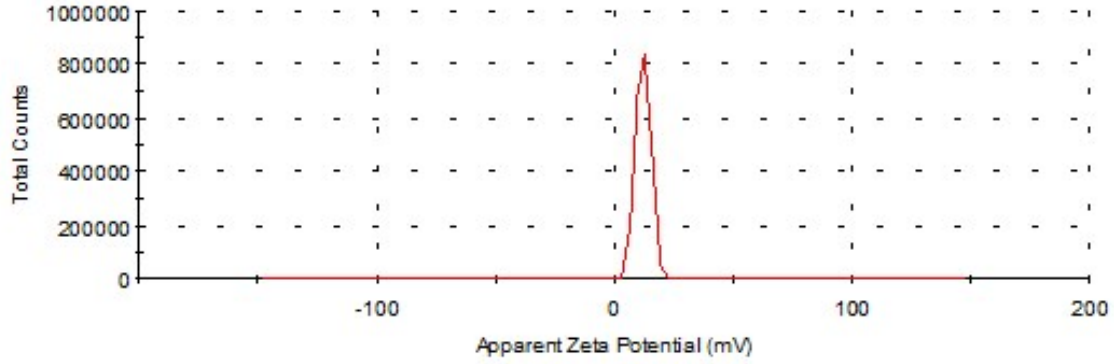

Fig. S32 Zeta potential result of **H⊃G** with an aqueous solution of 3.33×10^{-4} M.

10. Fluorescence spectroscopy study of the aggregation behavior

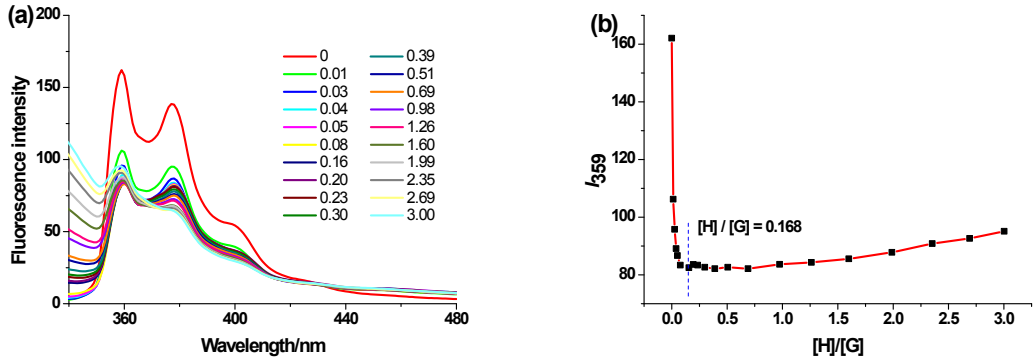

Fig. S33 (a) Fluorescence emission spectra of pyrene in aqueous solutions of **G** (80.0 μM) by increasing the concentration of **H** from 0 to 240 μM (0~3 equiv) at room temperature. (b) Dependence of the relative fluorescence intensity of pyrene on **H** concentration with a fixed concentration of **G** (80.0 μM) at room temperature. [pyrene] = 1.00 μM.

References:

S1. S. A. Caldarelli, S. E. Fangour, S. Wein, C. T. van Ba, C. Périgaud, A. Pellet, H. J. Vial and S. Peyrottes, *J. Med. Chem*., 2013, **56**, 496−509.

S2. (a) K. A. Connors, *Binding Constants, The Measurement of Molecular Complex Stability*, Wiley, New York, 1987; (b) P. R. Ashton, R. Ballardini, V. Balzani, M. Belohradsky, M. T. Gandolfi, D. Philp, L. Prodi, F. M. Raymo, M. V. Reddington, N. Spencer, J. F. Stoddart, M. Venturi and D. J. Williams, *J. Am. Chem. Soc*., 1996, **118**, 4931−4951; (c) Y. Inoue, K. Yamamoto, T. Wada, S. Everitt, X.-M. Gao, Z.-J. Hou, L.-H. Tong, S.-K. Jiang and H.-M. Wu, *J. Chem. Soc., Perkin Trans. 2*, 1998, 1807−1816.